Macromolecules

Article

Cite This: Macromolecules 2019, 52, 4847−4857

pubs.acs.org/Macromolecules

Engineering of Molecular Geometry in Bottlebrush Polymers

Dylan J. Walsh,[†] Sarit Dutta,[†] Charles E. Sing,*[,†,‡] and Damien Guironnet*[,†,‡]

[†]Department of Chemical and Biomolecular Engineering and [‡]Beckman Institute for Advanced Science and Technology, University of Illinois at Urbana−Champaign, Urbana, Illinois 61801, United States

Supporting Information

ABSTRACT: Bottlebrush polymers are large cylindrical macromolecules, where a molecular "width" emerges from a large number of side chains densely attached to a central backbone. The lengths of these grafted side chains exert indirect control over molecular flexibility, material processing, and molecular assembly behavior. Sequencing of the side-chain length is a promising route to further modify molecular geometry; however, tedious laboratory synthesis has imposed practical limits on this tunability. Here, we develop a methodology to overcome this limitation, leveraging automated synthesis and computer simulations to engineer bottlebrush polymers with three-dimensional molecular geometries. The automated flow synthesis platform combines fluid mechanics, reactor engineering, and living polymerization principles to gain precise synthetic control over the polymer architecture. Bottlebrush polymers with hourglass, football, bowtie, and sphere architecture profiles are synthesized with high molecular weights (up to 10^6 g mol^{-1}, ∼150 nm) and narrow dispersities ($Đ$ < 1.1). Atomic force microscopy and viscometry are used to illustrate the difference in the architecture of the polymers, providing results that match simulation predictions. This agreement enables the development of an inverse design protocol, where Monte Carlo simulations are used to correlate the molecular geometry for synthesis. This scalable synthetic strategy enables the production of *designer macromolecules* with *any* axisymmetric shape.

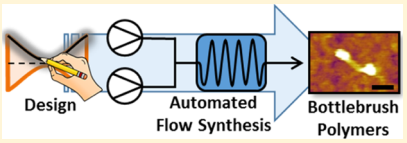

INTRODUCTION

The precise control over macromolecular chemical composition and shape is a hallmark of biological polymers. The hierarchical nature of biological structures gives rise to a wide variety of material properties and functionalities despite being built from a relatively small number of chemical building blocks (e.g., amino acids, base pairs, etc.).[1−4] The branched architectures of graft proteins, such as lubricin,[5] aggrecan,[6] and mucin,[7] play a major role in enabling their complex functionality. Mucins, for example, rely on their branched molecular architecture (layers of tethered brush- and gel-like mucins) to enable osmotic moduli gradients which aid in simultaneous mucus clearance and small molecule barrier properties.[8,9] We aspire to emulate biological control over macromolecular properties by enabling the molecular design of polymer architectures (repeat unit connectivity) and polymer three-dimensional (3D) geometries (equilibrium conformation in solution).

Automated synthesis is a paradigm shift in molecule production as it has significantly accelerated and simplified the access to a wide array of molecules with biology-like complexity.[10−13] This technological revolution is enabled by the development of laboratory-scale flow chemistry techniques, which are now being merged with the precision of living polymerizations. The primary structure of synthetic linear polymers (compositions, monomer sequences, molecular weights, and molecular weight distributions) can be precisely tuned *on-the-fly* using automated synthesis protocols.[14−16] However, the systematic control of the 3D *molecular geometry* of polymers remains to be addressed as it requires control of the polymer *architecture* (i.e., the length and connectivity between monomers) and predictive theoretical or computational models to link the architecture to the polymer *conformation* or *geometry* (i.e., the equilibrium spatial arrangement of these same monomers).

In this paper, we leverage the synergy between automated synthesis and computational simulations to create a methodology enabling the design and synthesis of polymers with precise macromolecular geometries (Figure 1). Our material platform is a class of highly branched polymers, known as bottlebrush polymers. These polymers adopt an elongated conformation and reduction in flexibility because of the steric repulsion among the side chains densely grafted to a molecular backbone.[17−30] Generally, bottlebrush polymers possess a cylindrical molecular geometry, with the side chains giving rise to a "width" dimension and the backbone size translating to a "length". A number of applications have benefited from the "semiflexible" rigid rod character of bottlebrush polymers: ultrasoft elastomers[17,31−36] enabled by low cross-linking density and diminished conformational degrees of freedom and self-assembled structures (photonic crystals,[35,37−49] drug delivery vehicles,[50−63] etc.) with rapid assembly rates because of the suppression of molecular entanglements.[64] These polymers are attractive as a platform for *designer macromolecules* because the bottlebrush width can be indirectly controlled via synthesis through variation of the side-chain length. Recent efforts have expanded the scope of accessible architectures beyond a simple cylindrical geometry; however, they have

Received: April 24, 2019
Revised: May 29, 2019
Published: June 20, 2019

DOI: 10.1021/acs.macromol.9b00845
Macromolecules 2019, 52, 4847−4857

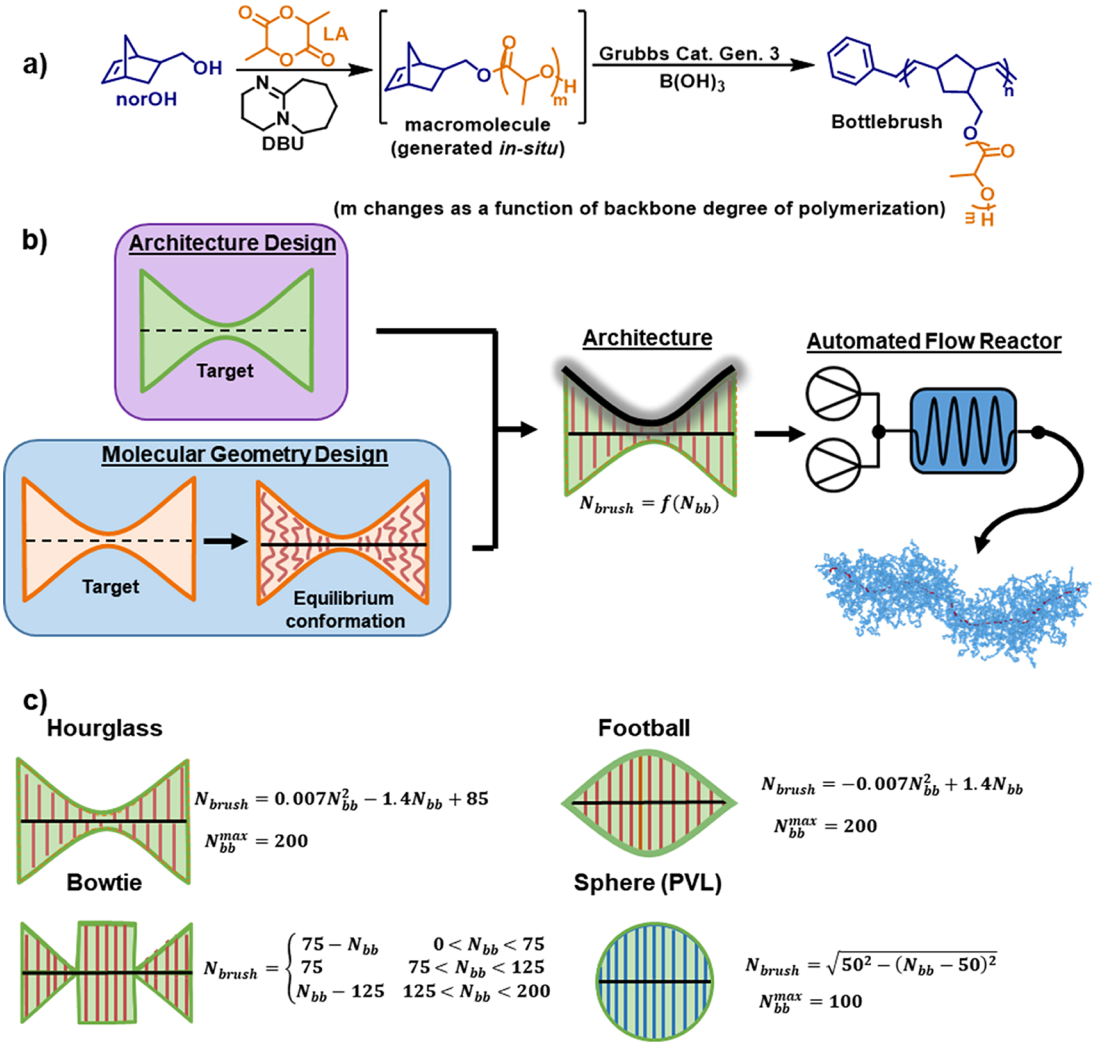

Figure 1. Overview of chemistry, design process, and design architectures. (a) Graft through synthesis of architecture-controlled bottlebrush polymers utilizing ROP of LA to produce macromonomers which are subsequently polymerized by third-generation Grubbs catalysts via ROMP. (b) Design workflow for the synthesis of bottlebrush. The upper route implements the targeted design directly to the architecture, whereas the bottom route implements an inverse design protocol to determine the architecture needed to produce a targeted molecular geometry. (c) Targeted bottlebrush architectures with the corresponding mathematical function synthesized in this manuscript.

suffered from tedious multistep synthesis or limited architecture control.[65−74] New advances are required to overcome these practical synthetic limitations, including our prior work which is limited to monotonic changes in branch length. Moreover, these methods have dealt solely with architecture control and have not translated to the equilibrium space-filling polymer conformation, that is, molecular geometry. Addressing this challenge requires advances in polymer modeling; classical polymer theories on linear and branched architectures[75−79] and more recent efforts considering bottlebrush architectures,[26−28,80−83] focus on how molecular size and shape emerge from monomer connectivity. An inverse relationship for how monomers should be connected to yield a desired molecular size and shape is instead required to *design* shape-defined bottlebrush molecules.

The automated synthesis platform reported here gives access to molecules with *any* axisymmetric geometry from commercially available reagents. The flexibility of this approach is illustrated by synthesizing hourglass, football, spherical, and bowtie architectures using two different polymer brushes (polylactic acid and polyvalerolactone) (Figure 1). The precision of the synthesis is illustrated through kinetics, atomic force microscopy (AFM), and viscometry experiments. The agreement between simulation predictions and experiments enables an inverse design protocol where molecular geometry is the target. The simplicity and high productivity of this strategy will accelerate the access to polymers with *3D molecular structures* and provide a unique platform to emulate the structure function relationships observed in biological polymers.

RESULTS AND DISCUSSION

The first section outlines the methodology, chemistry, and automated flow reactor development. This is followed by the implementation and validation of the automated flow system to produce macromonomers. Subsequently, the synthesis of architecture-controlled bottlebrush polymers was performed and validated by imaging and viscometry measurements in conjunction with simulations. The final section leverages a Monte Carlo simulation to implement an inverse design protocol to calculate the architecture necessary to produce any specific axisymmetric molecular geometry.

DOI: 10.1021/acs.macromol.9b00845
Macromolecules 2019, 52, 4847−4857

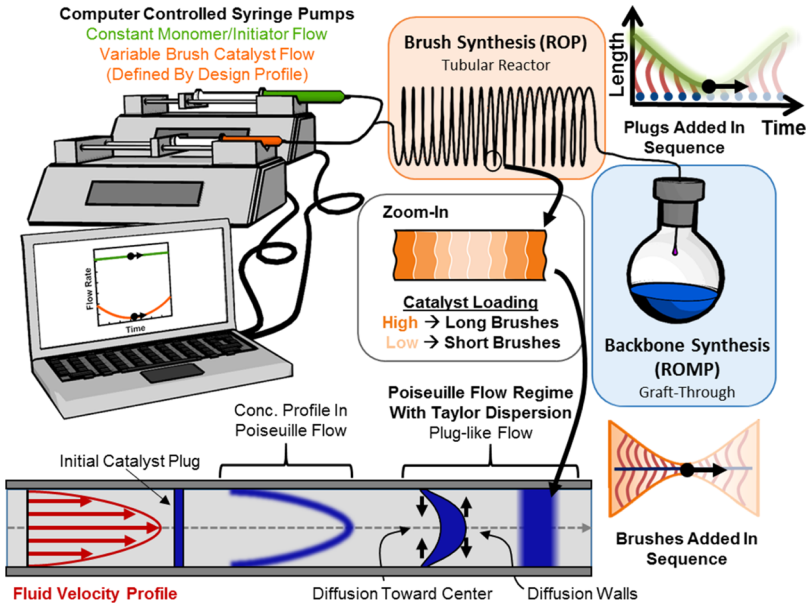

Figure 2. Automated flow reactor with bottlebrush synthesis and fluid mechanical elements. The setup consists of two computer-controlled syringe pumps connected to a long tubular reactor feeding into a collection pot. The green syringe contains the monomer and the initiator for the macromonomer synthesis and will flow at a constant rate. The orange syringe contains the catalyst and will flow at a variable rate defined by the design. The two solutions mix and enter the tubular reactor where the brush synthesis occurs. A zoom-in of the tubular reactor is present in the center of the figure detailing how each plug of fluid contains a different amount of catalyst. The higher the catalyst loading, the longer the brushes will be, and vice versa for low catalyst loading. The bottom of the figure provides a fluid mechanical description of the velocity profile (red), the initial catalyst plug, Poiseuille concentration profile without diffusion, and Poiseuille concentration profile with diffusion, where the blue color represents a single catalyst plug. The top right corner depicts the change in brush length as a function of time for an hourglass synthesis. The collection flask is where the brushes are added to a growing backbone via graft-through polymerization completing the synthesis of the architecture-controlled bottlebrush polymers.

Automated Flow Reactor Design. Bottlebrush polymers are produced in a two-step process where macromonomers are synthesized and then polymerized (graft-through polymerization).[18,38,57,67,80−87] We hypothesized that the bottlebrush polymers with any axisymmetric architecture can be accessed by synthesizing macromonomers of tunable length in a tubular flow reactor and slowly feeding them into a second batch reactor where they are polymerized in the desired sequence (Figure 2). This methodology relies on two polymerizations, macromonomer synthesis and backbone synthesis, being chemically compatible and orthogonal. An additional requirement is the nearly instantaneous incorporation of the slowly added macromonomers into the bottlebrush structure to avoid scrambling of macromonomers. We have previously identified the cascade ring-opening polymerization (ROP) of cyclic esters for the synthesis of the brushes and ring opening metathesis polymerization (ROMP) of norbornene-terminated macromonomer initiated by a ruthenium-based catalyst (Grubbs' third-generation catalyst, G3) for the backbone synthesis to satisfy all synthetic requirements.[67,88−91]

The synthesis of bottlebrush polymers with any axisymmetric architecture relies on the ability to precisely synthesize macromonomers of any length in a designed sequence. Per our hypothesis, we postulated that this control could be achieved by operating a computer-programmed flow reactor, where short plugs of fluid would form with different brush lengths because of different polymerization rates (Figure 2: zoom in). Turbulent flow regime (high Reynolds numbers) is the most common approach for producing plug flow; however, this is often impractical for laboratory scale as it requires the usage of large amounts of chemicals.[16,92] In contrast, laminar flow regime (low Reynolds numbers) can be easily implemented; however, this flow regime produces a parabolic velocity profile within the tube which causes a heterogeneity in residence time.[92] Nevertheless, when slow flow rates, narrow tube diameters, and long tube lengths are implemented, it is possible to enter a Poiseuille flow regime where Taylor dispersion leads to plugs.[93−101] This regime occurs when radial diffusion becomes significant over the reactor length (Figure 2: bottom).

To confirm that the automated flow reactor is capable of varying the macromonomer length *on-the-fly*, we performed the catalytic ROP of lactide (LA) and δ-valerolactone (VL) in the flow reactor without performing the subsequent graft-through polymerization of the backbone.[18,38,67,80−87] The reactor setup consists of two computer-controlled syringe pumps: one syringe pump flowing the monomer/initiator solution and the other flowing the catalyst solution into a long and narrow tubular reactor (7.62 m with a 0.508 mm inside diameter; see Supporting Information Section 2 for more details). The use of computer-controlled syringe pumps enables the automation and is a necessity to achieve the precise control over the polymer architecture. The degree of polymerization, which we correlate to the polymerization rate, can be controlled in the tubular reactor by varying the catalyst flow rate while maintaining a constant monomer/initiator flow rate. This designates the catalyst flow rate as the defining parameter of our process, where plugs containing high catalyst concentration will result in the formation of long macromonomers, whereas plugs with low catalyst concentration will yield short macromonomers.

DOI: 10.1021/acs.macromol.9b00845
Macromolecules 2019, 52, 4847−4857

The synthesis of any specific architecture requires a relationship between the targeted architecture profile (design parameter) and the catalyst flow rate (process parameter). Two independent approaches to correlate the catalyst flow rate with the macromonomer length were developed, as each method has its own merits. Method 1 implements the rate law for monomer consumption. A derivation using a general rate law that applies to most well-controlled polymerizations (eq 1),[102,103] tubular reactor design equations,[104,105] and the targeted architecture profile "f" (design profile) was performed to generate eq 2 (Supporting Information Section 4). The catalyst flow rate (Q_{syn2}, process parameter) can be calculated with eq 2 using a root-finding algorithm (a MATLAB code containing the secant method is provided in Supporting Information Section 12), and rate orders (a, b, c) can be determined from batch kinetics.

$$\frac{\mathrm{d[M]}}{\mathrm{d}t} = -k[\mathrm{I}]^a[\mathrm{cat}]^b[\mathrm{M}]^c \tag{1}$$

$$\frac{Q_{\mathrm{syn2}}{}^{b}}{(Q_{\mathrm{syn1}} + Q_{\mathrm{syn2}})^{a+b+c}} = -\frac{F_{\mathrm{M,o}}{}^{1-c}}{(c-1)(\pi R^2)Lk F_{\mathrm{I}}^{a}[\mathrm{cat}_{\mathrm{syn2}}]^b} \left(1 - \left(1 - \frac{f\left(\frac{[I_{\mathrm{syn1}}]Q_{\mathrm{syn1}}t}{n_{\mathrm{bb,cat}}}\right)}{N_{\mathrm{brush}}^{\mathrm{synmax}}}\right)^{1-c}\right) \tag{2}$$

To demonstrate the ability of method 1 to control the polymer length, three different architecture profiles (hourglass, football, and bowtie) were targeted by implementing the ROP of LA catalyzed by 8-diazabicyclo[5.4.0]undec-7-ene (DBU). In tetrahydrofuran (THF), the ROP of LA produces the reaction orders of a = 1, b = 1, and c = 1.8 (see Supporting Information Section 3, experimental details). For our experiments, a monomer/initiator solution ([LA] = 0.92 M, [LA]/[norOH] = 70), a catalyst solution ([DBU] = 0.3 M), a monomer/initiator flow rate of 0.125 mL min^{-1}, and a variable catalyst flow rate were used. Drops of the ROP reaction mixture were collected at the exit of the tubular reactor, quenched, and analyzed by gel permeation chromatography (GPC) to determine the polymer molecular weight and dispersity ($Đ$). Figure 3 details the results for the hourglass profile, in which the observed polymer molecular weights were in very close agreement with the targeted molecular weights. Additionally, narrow molecular weight distributions ($Đ$ < 1.10) were achieved, establishing the success and precision of the polymerization. Flow ROP with a football and a bowtie architecture profile also resulted in good agreement of the experimental brush length with theory (Figures S13 and S19). It is worth noting that the bowtie profile contains a brush length step change of 75 repeat units, which occurred over 1.4% of macromonomer solution, highlighting the resolution that can be achieved without the loss of molecular weight control. Overall, method 1 has the advantage that it remains valid with the changes in the experimental setup (reagent concentration or reactor size), but it requires the rate law of the polymerization to be known.

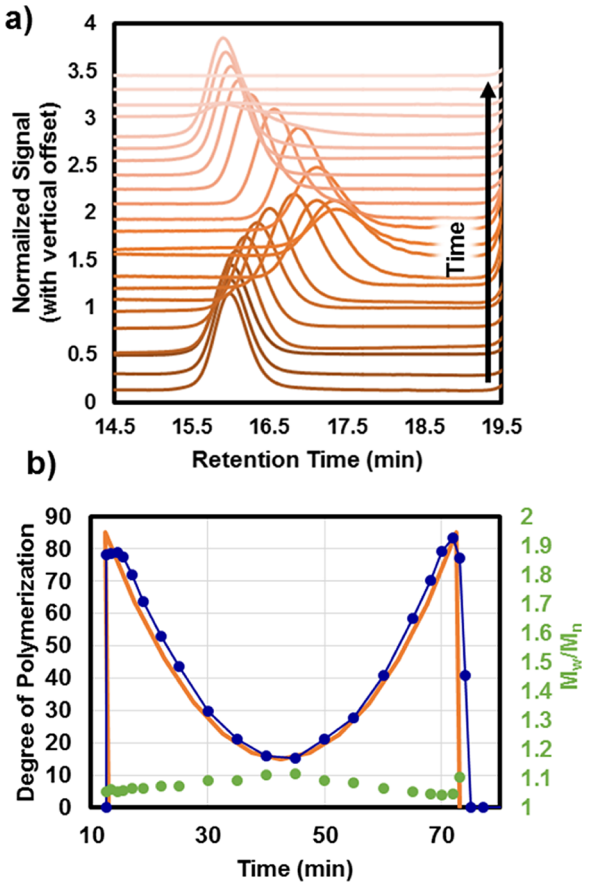

Figure 3. Demonstration of the ability of method 1 to relate a targeted architecture profile to the catalyst flow rate for the ROP of LA with an hourglass profile. (a) Stacked overlay of GPC chromatogram of aliquots exiting a single flow experiment showing the change in macromonomer molecular weight exiting the tubular reactor at different time points. (b) Data of the degree of polymerization and dispersity of the aliquots collected over time, revealing good agreement with the theoretical molecular weight predictions while maintaining a narrow molecular weight distribution. The orange line is the theoretical brush length profile, the blue dots are brush length calculated from GPC, and the green dots are molecular weight dispersity.

An alternative strategy, method 2, was developed when the polymerization rate law is not known. Method 2 is based on an empirical relationship between the degree of polymerization and catalyst loading for a fixed monomer concentration and a set range of catalyst concentrations. This relationship is experimentally determined in a single flow experiment where multiple different catalyst flow rates are run consecutively, and the resulting polymers are analyzed by GPC. By operating in the Poiseuille flow regime, where the Taylor dispersion is significant,[93−101] step changes in the catalyst flow rate result in step changes in the degree of polymerization while maintaining narrow dispersities. Each flow rate becomes a data point for the relationship between the catalyst flow rate and the macromonomer length, and a function is fitted between all the data points (Figure 4a, Supporting Information Section 8). This function can then be used to convert any architecture profile (design parameter) to the ROP catalyst flow rate (process parameter). The ROP of VL catalyzed by 1,5,7-triazabicyclo[4.4.0]dec-5-ene (TBD) was performed to illustrate method 2. We obtained a linear relationship between the

DOI: 10.1021/acs.macromol.9b00845
Macromolecules 2019, 52, 4847−4857

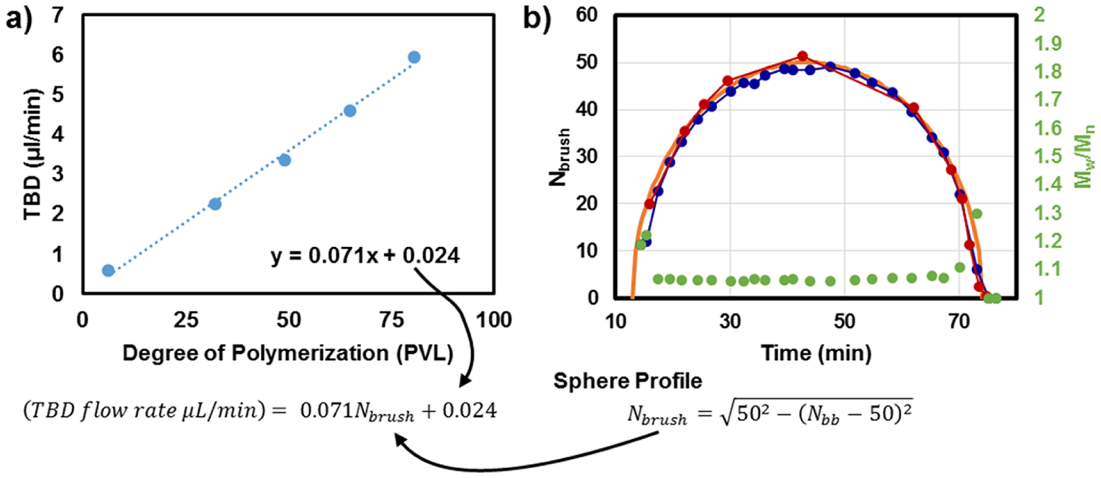

Figure 4. Demonstration of the ability of method 2 to relate a targeted architecture profile to the catalyst flow rate for the ROP of VL with a sphere profile. (a) Data for determining the empirical relationship between the degree of polymerization and catalyst loading via method 2. (b) Data of aliquots collected exiting the tubular reactor for the ROP of VL with a spherical profile. The orange line is the theoretical brush length profile, the red dots are brush length calculated from ^{1}H NMR, the blue dots are brush length calculated from GPC, and the green dots are molecular weight dispersity.

degree of polymerization and catalyst flow rates, but any function that describes the data can be used. The linear relationship was implemented to convert a spherical design profile into a TBD flow rate profile. The targeted and measured molecular weights were in very strong agreement, confirming the success of the methodology (Figure 4b). Overall, method 2 is faster and simpler to implement than method 1; however, any changes in the reactor, concentration, or monomer flow rates will require the determination of a new catalyst to degree of polymerization relationship.

Bottlebrush Synthesis and Characterization. Once the protocol for synthesizing macromonomers of various lengths with precise sequences was established, graft-through polymerization was added to the reactor setup to produce bottlebrush polymers. The synthesis of a polylactide (PLA) bottlebrush with an hourglass architecture was examined in detail by repeating the same experiment multiple times and rapidly quenching the ROMP reaction while simultaneously stopping the flow of macromonomers at different time points. The theoretical molecular weight of the bottlebrush polymer and the LA buildup (the unreacted LA that accumulates in the ROMP reaction vessel) can be calculated directly from the design equation and monomer molecular weights. ^{1}H nuclear magnetic resonance (NMR) of the aliquots provided the values for LA buildup and the residual levels of macromonomers present in solution, which were systematically below the detection limit (ROMP conversion > 98%,[67] Supporting Information Section 6). GPC of the same aliquots showed that the bottlebrush polymers had narrow molecular weight distributions ($Đ$ < 1.1), and most importantly, the measured molecular weights were in very close agreement with the theoretical molecular weights (Figure 5). The comparison of the experimental data with the corresponding theoretical values validates the success of the synthesis. The same hourglass bottlebrush was synthesized five times to yield 1.5 g of a bottlebrush polymer with a molecular weight standard deviation of 1.1%, showcasing the high reproducibility of the process (N_{BB} = 200, M_n = 744 kg/mol, $Đ$ = 1.08). The simplicity and versatility of the methodology were further illustrated by synthesizing bottlebrush polymers with football

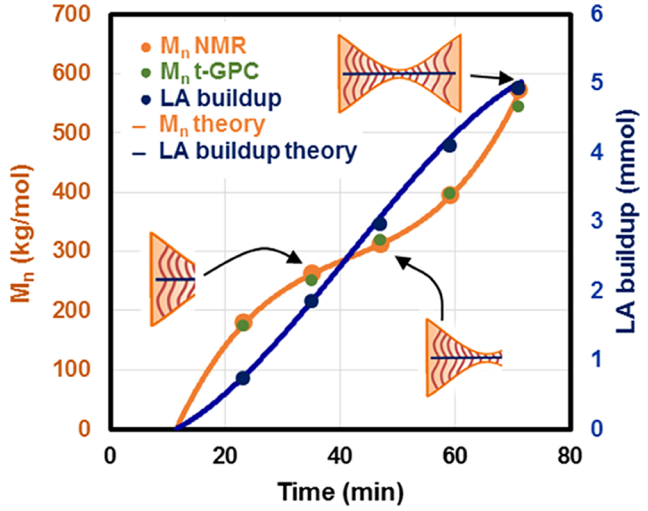

Figure 5. Molecular weight and LA buildup data for the synthesis of an hourglass bottlebrush. The data were obtained by performing the same synthesis multiple times and quenching the experiment at different time points for analysis. The lines are predictions calculated from the design equation and monomer molecular weights. The experimental data are represented by dots, in which M_n was obtained from ^{1}H NMR and triple detection GPC (t-GPC), and LA buildup was obtained from ^{1}H NMR.

and bowtie architecture profiles (Table 1). Finally, the chemical versatility was demonstrated by producing a poly(valerolactone) (PVL) bottlebrush with a spherical architecture (N_{BB} = 100, M_n = 379 kg/mol, $Đ$ = 1.05). In all cases, the bottlebrush polymers obtained had a narrow molecular weight distribution ($Đ$ < 1.15), no residual macromonomers were detected (GPC and ^{1}H NMR), and the molecular weights and cyclic ester buildup matched the theoretical values.

Visualization of the bottlebrush polymers was done using AFM[17,18,65,66,85,87,106−118] (Supporting Information Section 7). The images of hourglass bottlebrushes show two large ball ends connected by a thinner segment, which is consistent with the expectations of polymer conformations (Figure 6a). The measurement of the size of these molecular objects (~120 nm)

DOI: 10.1021/acs.macromol.9b00845
Macromolecules 2019, 52, 4847−4857

Table 1. Predicted and Experimental Data for the Synthesis of Architecture-Controlled Bottlebrush Polymers with N_{BB} = 200

		design and prediction			experimental data			
entry	brush polymer	architecture	LA/VL buildup (mmol)	M_n (kg/mol)	LA/VL buildup (mmol)[a]	conv. macro.[a] (%)	M_n (kg/mol)[b]	M_w/M_n[b]
1	PLA	hourglass	5.02	574	4.95	>98	546	1.07
2	PLA	football	4.60	699	4.55	>98	640	1.07
3	PLA	bowtie	4.60	698	4.58	>98	624	1.14
4	PVL	sphere	20.86	406	20.90	>98	379	1.05

[a]Calculated from conversion determined by ^{1}H NMR. [b]Calculated from t-GPC.

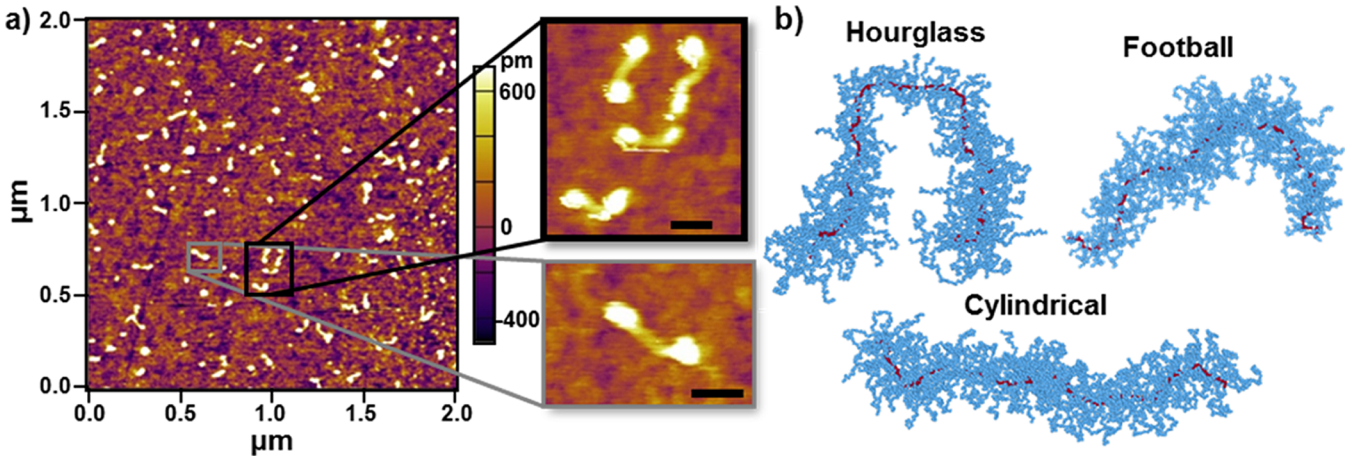

Figure 6. Images of architecture-controlled bottlebrush. (a) AFM images of hourglass bottlebrush polymers deposited on a silicon wafer with two zoomed-in images. The images depict polymers with two large ball ends connected by a thinner segment, consistent with the equilibrium conformations expected for an hourglass bottlebrush (scale bar = 50 nm). (b) Simulation snapshots of bottlebrush conformations for hourglass, football, and cylindrical architectures. Backbone beads are red and brush beads are blue. We are capable of visually observing the effect of different-length side chains on the bottlebrush conformations and note qualitative consistency between the hourglass conformation in simulation and the as-adsorbed conformations seen in AFM.

Table 2. Intrinsic Viscosity Data for Compositionally Identical Bottlebrushes (N_{BB} = 200)

	experiment[a]				simulation	
architecture	M_n[b] (kg/mol)	M_n/M_w[b]	$[\eta]$ (dL/g)	ratio[c]	$[\eta]$ dL/g	ratio[c]
hourglass	793	1.10	0.433	1.12	0.378	1.08
cylinder	768	1.03	0.387	1	0.349	1
football	811	1.05	0.318	0.82	0.282	0.81

[a]THF, 30 °C. [b]Calculated from t-GPC. [c]With respect to cylinder $[\eta]$.

and comparison to the theoretical length show that some contraction of the core occurs, which is consistent with the backbone flexibility decreasing with increasing brush length.

Simulation is a powerful tool for understanding bottlebrush conformation,[19,20,25−30,119−128] and our prior work has developed molecular simulation tools capable of quantitatively predicting the conformational structure of the synthesized bottlebrush molecules.[80] This same model is used to simulate architecture-controlled bottlebrush polymers (see Supporting Information Section 11). We show the snapshots of relaxed bottlebrush macromolecules calculated from Monte Carlo simulations in Figure 6b. The hourglass bottlebrush has short side chains in the center of the backbone contour, resulting in a higher flexibility of the backbone in the center. However, there is no apparent overall decrease in the backbone extension when compared to the cylindrical molecule. The snapshots of the hourglass architecture also qualitatively match with the AFM figures observed in Figure 6a. In contrast, the backbone at both ends of the football structure collapses toward the core because of the weak steric effects of the short side chains, which results in a shorter molecular length when compared to the cylindrical bottlebrush.

We have previously demonstrated that the equilibrium conformations obtained by the simulation procedure are capable of reproducing quantitative trends observed in the viscometry of a wide range of cylindrical bottlebrushes.[80] This prior work illustrates that intrinsic viscosity can be used as a sensitive probe of architecture to establish the quantitative aspect of the simulation. Therefore, intrinsic viscosity measurements were performed on an hourglass, a cylindrical, and a football bottlebrush with identical chemical composition (same backbone degree of polymerization and same average brush degree of polymerization) and compared with intrinsic viscosity calculations from equilibrium simulations.[129−132] Both methods showed that the hourglass bottlebrush has an intrinsic viscosity 10% larger when compared to a cylindrical bottlebrush. Conversely, the football bottlebrush has an intrinsic viscosity 20% smaller when compared to the cylindrical bottlebrush (Table 2). These results suggest that the football architecture takes a denser conformation in solution than the hourglass. This is further validated via the

DOI: 10.1021/acs.macromol.9b00845
Macromolecules 2019, 52, 4847−4857

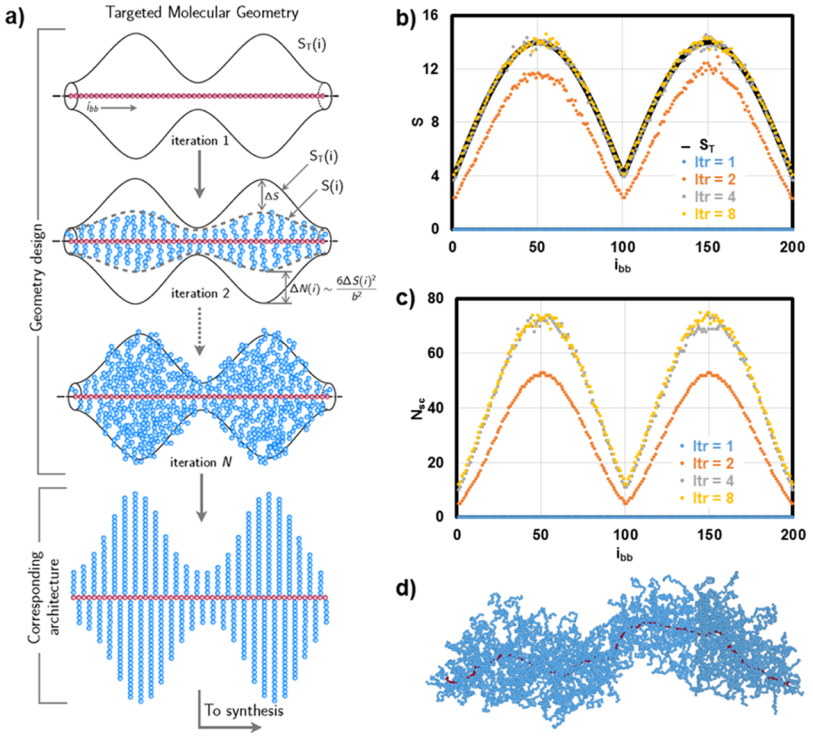

Figure 7. Inverse design scheme for bottlebrush geometry design. (a) Target width profile, the side-chain radius of gyration $S_T(i)$, is iteratively obtained by first taking a linear chain and adding $\Delta N(i)$ side-chain beads as a function of the index of the backbone monomer i. Subsequent iterations adjust this $\Delta N(i)$ based on the distance $\Delta S(i)$ of the width from the target, until convergence is obtained. The architectural information $N_{SC}(i)$ is an input to the synthesis, corresponding to the target molecular geometry. (b) Side-chain radius of gyration $S(i)$ as a function of iteration *itr* for an example geometry. Convergence to $S_T(i)$ is observed even after only four iterations. (c) Corresponding values of $N_{SC}(i)$ as a function of *itr*. We note that although there is a clear correspondence between the architecture $N_{SC}(i)$ and geometry $S_T(i)$, it is not proportional. (d) Simulation snapshot of the converged structure based on the inverse design protocol.

trends observed with their respective GPC elution times ($t_{peak}^{hourglass}$ = 12.61 ± 0.01 min and $t_{peak}^{football}$ = 12.73 ± 0.08 min). Overall, the simulation data provide an additional independent confirmation of the success of the architecture-controlled synthesis.

Inverse Design of Molecular Geometry. The quantitative prediction of the simulation regarding the molecular conformation in solution provides a powerful method to connect the architecture profile and molecular geometry. This sets the basis of an inverse design protocol[133−137] for calculating the bottlebrush architecture profile (process parameter) that must be synthesized to yield a specific molecular geometry (design parameter). We use the average radius of gyration $S = \langle R_{G,SC}^2 \rangle^{1/2}$ of a bottlebrush side chain as a descriptor of the bottlebrush "width",[80] which can vary as a function of the position i along the bottlebrush backbone contour, $S(i)$. The desired axisymmetric design profile is defined by a target function $S_T(i)$. The inverse design process begins with a bare backbone chain, and we iteratively remove or add side-chain beads to approach this targeted profile. The number of beads added onto or removed from the side chain ΔN is determined based on an error function $E(i) = S_T(i) - S(i)$, via the equation $6E^2(i)/b^2 = \Delta N$, which when converged yields an architectural profile $N_{SC}(i)$ for the degree of polymerization for each side chain. Figure 7 shows this process, plotting both the contour-dependent $N_{SC}(i)$ and $R_{G,SC}(i)$, with a double-sphere profile as the targeted molecular geometry. The first iteration is a straight line at $N_{SC}(i)$, representing the initial linear homopolymer. Subsequent iterations add and subtract lengths from the bottlebrush side chains, until a desired geometry $R_{G,SC}(i) \approx R_{G,T}(i)$ is found. The resulting architecture profile $N_{SC}(i)$ that leads to this geometric target $R_{G,T}(i)$ was subsequently used as an input to the automated flow synthesis, thereby allowing the engineering of macromolecules with controllable geometry (see Supporting Information Section 6). Significantly, we note that the desired molecular geometry and the architecture show similar trends but are not linearly proportional; this inverse design strategy enables the prediction of this nontrivial connection between the architecture and molecular geometry, which would otherwise be dependent not only on the side-chain length at a given location but also on the sequence of nearby side-chain lengths.

■ CONCLUSIONS

We have developed an automated methodology to synthesize macromolecules with 3D geometry. Our approach consists of performing a computer simulation to correlate molecular geometry to bottlebrush polymer architecture, followed by the synthesis of the predicted axisymmetric bottlebrush architecture. This synthetic achievement is enabled by the combination of the theoretical description provided by the simulation, the precise reactor engineering, and the living polymerizations employed. The simplicity, versatility, and productivity of using an automated flow reactor to control the polymer architecture will pave the way for rapid material design and lower the barrier for the synthesis of a large array of complex materials. Moreover, this methodology seeks to catalyze the establishment of new structure−function relationships in soft matter

DOI: 10.1021/acs.macromol.9b00845
Macromolecules 2019, 52, 4847−4857

with the aspiration of matching the specificity observed for biopolymers.

■ ASSOCIATED CONTENT

Supporting Information

The Supporting Information is available free of charge on the ACS Publications website at DOI: 10.1021/acs.macromol.9b00845.

Scheme of the reactor setup correlated back to the real-world reactor setup; Mn versus time and rate versus lactide concentration for the ROP of lactide with various amounts of DBU and OH; DBU flow rate and GPC chromatograms for the football, bowtie, and hourglass ROP of lactide; GPC chromatograms and ^{1}H NMR spectra of the bottlebrush kinetic aliquots; cylinder, hourglass, and football profiles with identical composition; schematic of the inverse design to obtain brush profile function; height map and normalized height profiles of hourglass and football bottlebrush polymers; brush length results, GPC traces, and ^{1}H NMR spectra for the TBD flow rate sweep; TBD flow rate profile for a sphere bottlebrush; GPC chromatograms and ^{1}H NMR spectra for the sphere ROP of valerolactone; GPC chromatograms and ^{1}H NMR spectra for the synthesis of PVL bottlebrush; and data for the calculation of intrinsic viscosity (PDF)

■ AUTHOR INFORMATION

Corresponding Authors

*E-mail: cesing@illinois.edu (C.E.S.).
*E-mail: guironne@illinois.edu (D.G.).

ORCID

Sarit Dutta: 0000-0002-6197-7881
Charles E. Sing: 0000-0001-7231-2685
Damien Guironnet: 0000-0002-0356-6697

Funding

The authors thank the NSF DMR 17-27605 for funding.

Notes

The authors declare no competing financial interest.

■ ACKNOWLEDGMENTS

PolyAnalytik Inc. (London, Canada) is acknowledged for performing triple detection gel permeation chromatography. Major funding for the 500 MHz Bruker CryoProbe was provided by the Roy J. Carver Charitable Trust to the School of Chemical Sciences NMR Lab. AFM was carried out at Frederick Seitz Materials Research Laboratory Central Research Facilities, University of Illinois. The authors thank Umicore for the generous gift of the Grubbs catalyst.

■ REFERENCES

(1) Matyjaszewski, K.; Tsarevsky, N. V. Nanostructured Functional Materials Prepared by Atom Transfer Radical Polymerization. *Nat. Chem.* **2009**, *1*, 276−288.
(2) Lutz, J.-F.; Lehn, J.-M.; Meijer, E. W.; Matyjaszewski, K. From Precision Polymers to Complex Materials and Systems. *Nat. Rev. Mater.* **2016**, *1*, 16024.
(3) Chen, C.; Wylie, R. A. L.; Klinger, D.; Connal, L. A. Shape Control of Soft Nanoparticles and Their Assemblies. *Chem. Mater.* **2017**, *29*, 1918.
(4) Mahon, C. S.; Fulton, D. A. Mimicking Nature with Synthetic Macromolecules Capable of Recognition. *Nat. Chem.* **2014**, *6*, 665−672.
(5) Lee, Y.; Choi, J.; Hwang, N. S. Regulation of Lubricin for Functional Cartilage Tissue Regeneration: A Review. *Biomater. Res.* **2018**, *22*, 9.
(6) Kiani, C.; Chen, L.; Wu, Y. J.; Yee, A. J.; Yang, B. B. Structure and Function of Aggrecan. *Cell Res* **2002**, *12*, 19−32.
(7) McGuckin, M. A.; Lindén, S. K.; Sutton, P.; Florin, T. H. Mucin Dynamics and Enteric Pathogens. *Nat. Rev. Microbiol.* **2011**, *9*, 265−278.
(8) Linden, S. K.; Sutton, P.; Karlsson, N. G.; Korolik, V.; McGuckin, M. A. Mucins in the mucosal barrier to infection. *Mucosal Immunol.* **2008**, *1*, 183−197.
(9) Button, B.; Cai, L. H.; Ehre, C.; Kesimer, M.; Hill, D. B.; Sheehan, J. K.; Boucher, R. C.; Rubinstein, M. A periciliary brush promotes the lung health by separating the mucus layer from airway epithelia. *Science* **2012**, *337*, 937−941.
(10) Li, T.; Liu, L.; Wei, N.; Yang, J.-Y.; Chapla, D. G.; Moremen, K. W.; Boons, G.-J. An Automated Platform for the Enzyme-Mediated Assembly of Complex Oligosaccharides. *Nat. Chem.* **2019**, *11*, 229−236.
(11) Trobe, M.; Burke, M. D. The Molecular Industrial Revolution: Automated Synthesis of Small Molecules. *Angew. Chem., Int. Ed.* **2018**, *57*, 4192−4214.
(12) Elvira, K. S.; I Solvas, X. C.; Wootton, R. C. R.; Demello, A. J. The Past, Present and Potential for Microfluidic Reactor Technology in Chemical Synthesis. *Nat. Chem.* **2013**, *5*, 905−915.
(13) Bédard, A.-C.; Adamo, A.; Aroh, K. C.; Russell, M. G.; Bedermann, A. A.; Torosian, J.; Yue, B.; Jensen, K. F.; Jamison, T. F. Reconfigurable System for Automated Optimization of Diverse Chemical Reactions. *Science* **2018**, *361*, 1220−1225.
(14) Rubens, M.; Vrijsen, J. H.; Laun, J.; Junkers, T. Precise Polymer Synthesis by Autonomous Self-Optimizing Flow Reactors. *Angew. Chem., Int. Ed.* **2019**, *58*, 3183−3187.
(15) Corrigan, N.; Almasri, A.; Taillades, W.; Xu, J.; Boyer, C. Controlling Molecular Weight Distributions through Photoinduced Flow Polymerization. *Macromolecules* **2017**, *50*, 8438−8448.
(16) Tonhauser, C.; Natalello, A.; Löwe, H.; Frey, H. Microflow Technology in Polymer Synthesis. *Macromolecules* **2012**, *45*, 9551−9570.
(17) Daniel, W. F. M.; Burdyńska, J.; Vatankhah-Varnoosfaderani, M.; Matyjaszewski, K.; Paturej, J.; Rubinstein, M.; Dobrynin, A. V.; Sheiko, S. S. Solvent-Free, Supersoft and Superelastic Bottlebrush Melts and Networks. *Nat. Mater.* **2016**, *15*, 183−189.
(18) Verduzco, R.; Li, X.; Pesek, S. L.; Stein, G. E. Structure, Function, Self-Assembly, and Applications of Bottlebrush Copolymers. *Chem. Soc. Rev.* **2015**, *44*, 2405−2420.
(19) Cao, Z.; Carrillo, J.-M. Y.; Sheiko, S. S.; Dobrynin, A. V. Computer Simulations of Bottle Brushes: From Melts to Soft Networks. *Macromolecules* **2015**, *48*, 5006−5015.
(20) Lyubimov, I.; Wessels, M. G.; Jayaraman, A. Molecular Dynamics Simulation and PRISM Theory Study of Assembly in Solutions of Amphiphilic Bottlebrush Block Copolymers. *Macromolecules* **2018**, *51*, 7586−7599.
(21) Zhulina, E. B.; Sheiko, S. S.; Borisov, O. V. Solution and Melts of Barbwire Bottlebrushes: Hierarchical Structure and Scale-Dependent Elasticity. *Macromolecules* **2019**, *52*, 1671−1684.
(22) Ober, C. K. POLYMER SCIENCE:Shape Persistence of Synthetic Polymers. *Science* **2000**, *288*, 448−449.
(23) Birshtein, T. M.; Borisov, O. V.; Zhulina, Y. B.; Khokhlov, A. R.; Yurasova, T. A. Conformations of Comb-like Macromolecules. *Polym. Sci. U.S.S.R.* **1987**, *29*, 1293−1300.
(24) Fredrickson, G. H. Surfactant-Induced Lyotropic Behavior of Flexible Polymer Solutions. *Macromolecules* **1993**, *26*, 2825−2831.
(25) Yethiraj, A. A Monte Carlo Simulation Study of Branched Polymers. *J. Chem. Phys.* **2006**, *125*, 204901.

DOI: 10.1021/acs.macromol.9b00845
Macromolecules 2019, 52, 4847−4857

(26) Hsu, H.-P.; Paul, W.; Binder, K. Structure of Bottle-Brush Polymers in Solution: A Monte Carlo Test of Models for the Scattering Function. *J. Chem. Phys.* **2008**, *129*, 204904.
(27) Hsu, H.-P.; Paul, W.; Binder, K. One- and Two-Component Bottle-Brush Polymers: Simulations Compared to Theoretical Predictions. *Macromol. Theory Simulations* **2007**, *16*, 660−689.
(28) Hsu, H.-P.; Paul, W.; Binder, K. Understanding the Multiple Length Scales Describing the Structure of Bottle-Brush Polymers by Monte Carlo Simulation Methods. *Macromol. Theory Simulations* **2011**, *20*, 510−525.
(29) Theodorakis, P. E.; Hsu, H.-P.; Paul, W.; Binder, K. Computer Simulation of Bottle-Brush Polymers with Flexible Backbone: Good Solvent versus Theta Solvent Conditions. *J. Chem. Phys.* **2011**, *135*, 164903.
(30) Hsu, H.-P.; Paul, W.; Rathgeber, S.; Binder, K. Characteristic Length Scales and Radial Monomer Density Profiles of Molecular Bottle-Brushes: Simulation and Experiment. *Macromolecules* **2010**, *43*, 1592−1601.
(31) Vatankhah-Varnosfaderani, M.; Daniel, W. F. M.; Everhart, M. H.; Pandya, A. A.; Liang, H.; Matyjaszewski, K.; Dobrynin, A. V.; Sheiko, S. S. Mimicking Biological Stress-Strain Behaviour with Synthetic Elastomers. *Nature* **2017**, *549*, 497−501.
(32) Liang, H.; Sheiko, S. S.; Dobrynin, A. V. Supersoft and Hyperelastic Polymer Networks with Brushlike Strands. *Macromolecules* **2018**, *51*, 638−645.
(33) Vatankhah-Varnoosfaderani, M.; Daniel, W. F. M.; Zhushma, A. P.; Li, Q.; Morgan, B. J.; Matyjaszewski, K.; Armstrong, D. P.; Spontak, R. J.; Dobrynin, A. V.; Sheiko, S. S. Bottlebrush Elastomers: A New Platform for Freestanding Electroactuation. *Adv. Mater.* **2017**, *29*, 1604209.
(34) Sarapas, J. M.; Chan, E. P.; Rettner, E. M.; Beers, K. L. Compressing and Swelling to Study the Structure of Extremely Soft Bottlebrush Networks Prepared by ROMP. *Macromolecules* **2018**, *51*, 2359−2366.
(35) Vatankhah-Varnosfaderani, M.; Keith, A. N.; Cong, Y.; Liang, H.; Rosenthal, M.; Sztucki, M.; Clair, C.; Magonov, S.; Ivanov, D. A.; Dobrynin, A. V.; et al. Chameleon-like Elastomers with Molecularly Encoded Strain-Adaptive Stiffening and Coloration. *Science* **2018**, *359*, 1509−1513.
(36) Xie, G.; Martinez, M. R.; Olszewski, M.; Sheiko, S. S.; Matyjaszewski, K. Molecular Bottlebrushes as Novel Materials. *Biomacromolecules* **2019**, *20*, 27−54.
(37) Boyle, B. M.; French, T. A.; Pearson, R. M.; McCarthy, B. G.; Miyake, G. M. Structural Color for Additive Manufacturing: 3D-Printed Photonic Crystals from Block Copolymers. *ACS Nano* **2017**, *11*, 3052−3058.
(38) Lin, T.-P.; Chang, A. B.; Luo, S.-X.; Chen, H.-Y.; Lee, B.; Grubbs, R. H. Effects of Grafting Density on Block Polymer Self-Assembly: From Linear to Bottlebrush. *ACS Nano* **2017**, *11*, 11632−11641.
(39) Song, D.-P.; Li, C.; Li, W.; Watkins, J. J. Block Copolymer Nanocomposites with High Refractive Index Contrast for One-Step Photonics. *ACS Nano* **2016**, *10*, 1216−1223.
(40) Song, D.-P.; Jacucci, G.; Dundar, F.; Naik, A.; Fei, H. F.; Vignolini, S.; Watkins, J. J. Photonic Resins: Designing Optical Appearance via Block Copolymer Self-Assembly. *Macromolecules* **2018**, *51*, 2395−2400.
(41) Runge, M. B.; Bowden, N. B. Synthesis of High Molecular Weight Comb Block Copolymers and Their Assembly into Ordered Morphologies in the Solid State. *J. Am. Chem. Soc.* **2007**, *129*, 10551−10560.
(42) Miyake, G. M.; Piunova, V. A.; Weitekamp, R. A.; Grubbs, R. H. Precisely Tunable Photonic Crystals From Rapidly Self-Assembling Brush Block Copolymer Blends. *Angew. Chem., Int. Ed.* **2012**, *51*, 11246−11248.
(43) Macfarlane, R. J.; Kim, B.; Lee, B.; Weitekamp, R. A.; Bates, C. M.; Lee, S. F.; Chang, A. B.; Delaney, K. T.; Fredrickson, G. H.; Atwater, H. A.; et al. Improving Brush Polymer Infrared One-Dimensional Photonic Crystals via Linear Polymer Additives. *J. Am. Chem. Soc.* **2014**, *136*, 17374−17377.
(44) Sveinbjornsson, B. R.; Weitekamp, R. A.; Miyake, G. M.; Xia, Y.; Atwater, H. A.; Grubbs, R. H. Rapid Self-Assembly of Brush Block Copolymers to Photonic Crystals. *Proc. Natl. Acad. Sci. U.S.A.* **2012**, *109*, 14332−14336.
(45) Liberman-Martin, A. L.; Chu, C. K.; Grubbs, R. H. Application of Bottlebrush Block Copolymers as Photonic Crystals. *Macromol. Rapid Commun.* **2017**, *38*, 1700058.
(46) Song, D.-P.; Zhao, T. H.; Guidetti, G.; Vignolini, S.; Parker, R. M. Hierarchical Photonic Pigments via the Confined Self-Assembly of Bottlebrush Block Copolymers. *ACS Nano* **2019**, *13*, 1764−1771.
(47) Rzayev, J. Synthesis of Polystyrene−Polylactide Bottlebrush Block Copolymers and Their Melt Self-Assembly into Large Domain Nanostructures. *Macromolecules* **2009**, *42*, 2135−2141.
(48) Chae, C.-G.; Yu, Y.-G.; Seo, H.-B.; Kim, M.-J.; Grubbs, R. H.; Lee, J.-S. Experimental Formulation of Photonic Crystal Properties for Hierarchically Self-Assembled POSS-Bottlebrush Block Copolymers. *Macromolecules* **2018**, *51*, 3458−3466.
(49) Miyake, G. M.; Weitekamp, R. A.; Piunova, V. A.; Grubbs, R. H. Synthesis of Isocyanate-Based Brush Block Copolymers and Their Rapid Self-Assembly to Infrared-Reflecting Photonic Crystals. *J. Am. Chem. Soc.* **2012**, *134*, 14249−14254.
(50) Zeng, X.; Wang, L.; Liu, D.; Liu, D. Poly(L-Lysine)-Based Cylindrical Copolypeptide Brushes as Potential Drug and Gene Carriers. *Colloid Polym. Sci.* **2016**, *294*, 1909−1920.
(51) Müllner, M. Molecular Polymer Brushes in Nanomedicine. *Macromol. Chem. Phys.* **2016**, *217*, 2209−2222.
(52) Sowers, M. A.; Mccombs, J. R.; Wang, Y.; Paletta, J. T.; Morton, S. W.; Dreaden, E. C.; Boska, M. D.; Francesca Ottaviani, M.; Hammond, P. T.; Rajca, A.; et al. Redox-Responsive Branched-Bottlebrush Polymers for in Vivo MRI and Fluorescence Imaging. *Nat. Commun.* **2014**, *5*, 5460.
(53) Ding, D.; Li, K.; Zhu, Z.; Pu, K.-Y.; Hu, Y.; Jiang, X.; Liu, B. Conjugated Polyelectrolyte-Cisplatin Complex Nanoparticles for Simultaneous in Vivo Imaging and Drug Tracking. *Nanoscale* **2011**, *3*, 1997−2002.
(54) Huang, K.; Rzayev, J. Well-Defined Organic Nanotubes from Multicomponent Bottlebrush Copolymers. *J. Am. Chem. Soc.* **2009**, *131*, 6880−6885.
(55) Huang, K.; Jacobs, A.; Rzayev, J. De Novo Synthesis and Cellular Uptake of Organic Nanocapsules with Tunable Surface Chemistry. *Biomacromolecules* **2011**, *12*, 2327−2334.
(56) Yang, T.; Liu, L.; Deng, Y.; Guo, Z.; Zhang, G.; Ge, Z.; Ke, H.; Chen, H. Ultrastable Near-Infrared Conjugated-Polymer Nanoparticles for Dually Photoactive Tumor Inhibition. *Adv. Mater.* **2017**, *29*, 1700487.
(57) Miki, K.; Kimura, A.; Oride, K.; Kuramochi, Y.; Matsuoka, H.; Harada, H.; Hiraoka, M.; Ohe, K. High-Contrast Fluorescence Imaging of Tumors in Vivo Using Nanoparticles of Amphiphilic Brush-like Copolymers Produced by ROMP. *Angew. Chem., Int. Ed.* **2011**, *50*, 6567−6570.
(58) Liao, L.; Liu, J.; Dreaden, E. C.; Morton, S. W.; Shopsowitz, K. E.; Hammond, P. T.; Johnson, J. A. A Convergent Synthetic Platform for Single-Nanoparticle Combination Cancer Therapy: Ratiometric Loading and Controlled Release of Cisplatin, Doxorubicin, and Camptothecin. *J. Am. Chem. Soc.* **2014**, *136*, 5896−5899.
(59) Shen, Y.; Zhan, Y.; Tang, J.; Xu, P.; Johnson, P. A.; Radosz, M.; Van Kirk, E. A.; Murdoch, W. J. Multifunctioning PH-Responsive Nanoparticles from Hierarchical Self-Assembly of Polymer Brush for Cancer Drug Delivery. *AIChE J.* **2008**, *54*, 2979−2989.
(60) Zou, J.; Jafr, G.; Cheng, C.; Themistou, E.; Yap, Y.; Wintrob, Z. A. P.; Alexandridis, P.; Ceacareanu, A. C. PH-Sensitive Brush Polymer-Drug Conjugates by Ring-Opening Metathesis Copolymerization. *Chem. Commun.* **2011**, *47*, 4493.
(61) Zou, J.; Yu, Y.; Li, Y.; Ji, W.; Chen, C.-K.; Law, W.-C.; Prasad, P. N.; Cheng, C. Well-defined diblock brush polymer-drug conjugates for sustained delivery of paclitaxel. *Biomater. Sci.* **2015**, *3*, 1078−1084.

DOI: 10.1021/acs.macromol.9b00845
Macromolecules 2019, 52, 4847−4857

(62) Johnson, J. A.; Lu, Y. Y.; Burts, A. O.; Xia, Y.; Durrell, A. C.; Tirrell, D. A.; Grubbs, R. H. Drug-Loaded, Bivalent-Bottle-Brush Polymers by Graft-through ROMP. *Macromolecules* **2010**, *43*, 10326−10335.
(63) Lu, X.; Tran, T.-H.; Jia, F.; Tan, X.; Davis, S.; Krishnan, S.; Amiji, M. M.; Zhang, K. Providing Oligonucleotides with Steric Selectivity by Brush-Polymer-Assisted Compaction. *J. Am. Chem. Soc.* **2015**, *137*, 12466−12469.
(64) Namba, S.; Tsukahara, Y.; Kaeriyama, K.; Okamoto, K.; Takahashi, M. Bulk Properties of Multibranched Polystyrenes from Polystyrene Macromonomers: Rheological Behavior I. *Polymer* **2000**, *41*, 5165−5171.
(65) Li, A.; Li, Z.; Zhang, S.; Sun, G.; Policarpio, D. M.; Wooley, K. L. Synthesis and Direct Visualization of Dumbbell-Shaped Molecular Brushes. *ACS Macro Lett.* **2012**, *1*, 241−245.
(66) Radzinski, S. C.; Foster, J. C.; Scannelli, S. J.; Weaver, J. R.; Arrington, K. J.; Matson, J. B. Tapered Bottlebrush Polymers: Cone-Shaped Nanostructures by Sequential Addition of Macromonomers. *ACS Macro Lett.* **2017**, *6*, 1175−1179.
(67) Walsh, D. J.; Guironnet, D. Macromolecules with Programmable Shape, Size, and Chemistry. *Proc. Natl. Acad. Sci. U.S.A.* **2019**, *116*, 1538−1542.
(68) Yavitt, B. M.; Fei, H.-F.; Kopanati, G. N.; Winter, H. H.; Watkins, J. J. Power Law Relaxations in Lamellae Forming Brush Block Copolymers with Asymmetric Molecular Shape. *Macromolecules* **2019**, *52*, 1557−1566.
(69) Gai, Y.; Song, D.-P.; Yavitt, B. M.; Watkins, J. J. Polystyrene-block-poly(ethylene oxide) Bottlebrush Block Copolymer Morphology Transitions: Influence of Side Chain Length and Volume Fraction. *Macromolecules* **2017**, *50*, 1503−1511.
(70) Fenyves, R.; Schmutz, M.; Horner, I. J.; Bright, F. V.; Rzayev, J. Aqueous Self-Assembly of Giant Bottlebrush Block Copolymer Surfactants as Shape-Tunable Building Blocks. *J. Am. Chem. Soc.* **2014**, *136*, 7762−7770.
(71) Jha, S.; Dutta, S.; Bowden, N. B. Synthesis of Ultralarge Molecular Weight Bottlebrush Polymers Using Grubbs' Catalysts. *Macromolecules* **2004**, *37*, 4365−4374.
(72) Shi, Y.; Zhu, W.; Yao, D.; Long, M.; Peng, B.; Zhang, K.; Chen, Y. Disk-Like Micelles with a Highly Ordered Pattern from Molecular Bottlebrushes. *ACS Macro Lett.* **2013**, *3*, 70−73.
(73) Xiao, L.; Qu, L.; Zhu, W.; Wu, Y.; Liu, Z.; Zhang, K. Donut-Shaped Nanoparticles Templated by Cyclic Bottlebrush Polymers. *Macromolecules* **2017**, *50*, 6762−6770.
(74) Huang, K.; Canterbury, D. P.; Rzayev, J. Synthesis of Segmented Polylactide Molecular Brushes and Their Transformation to Open-End Nanotubes. *Macromolecules* **2010**, *43*, 6632−6638.
(75) Theodorou, D. N.; Suter, U. W. Shape of Unperturbed Linear Polymers: Polypropylene. *Macromolecules* **1985**, *18*, 1206−1214.
(76) Alim, K.; Frey, E. Shapes of Semiflexible Polymer Rings. *Phys. Rev. Lett.* **2007**, *99*, 198102.
(77) Šolc, K.; Stockmayer, W. H. Shape of a Random-Flight Chain. *J. Chem. Phys.* **1971**, *54*, 2756−2757.
(78) Zimm, B. H.; Stockmayer, W. H. The Dimensions of Chain Molecules Containing Branches and Rings. *J. Chem. Phys.* **1949**, *17*, 1301−1314.
(79) Daoud, M.; Cotton, J. P. Star Shaped Polymers: A Model for the Conformation and Its Concentration Dependence. *J. Phys.* **1982**, *43*, 531.
(80) Dutta, S.; Wade, M. A.; Walsh, D. J.; Guironnet, D.; Rogers, S. A.; Sing, C. E. Dilute solution structure of bottlebrush polymers. *Soft Matter* **2019**, *15*−2941. DOI: 10.1039/c9sm00033j
(81) Lin, T.-P.; Chang, A. B.; Chen, H.-Y.; Liberman-Martin, A. L.; Bates, C. M.; Voegtle, M. J.; Bauer, C. A.; Grubbs, R. H. Control of Grafting Density and Distribution in Graft Polymers by Living Ring-Opening Metathesis Copolymerization. *J. Am. Chem. Soc.* **2017**, *139*, 3896−3903.
(82) Xu, B.; Feng, C.; Huang, X. A Versatile Platform for Precise Synthesis of Asymmetric Molecular Brush in One Shot. *Nat. Commun.* **2017**, *8*, 333.
(83) Chang, A. B.; Lin, T.-P.; Thompson, N. B.; Luo, S.-X.; Liberman-Martin, A. L.; Chen, H.-Y.; Lee, B.; Grubbs, R. H. Design, Synthesis, and Self-Assembly of Polymers with Tailored Graft Distributions. *J. Am. Chem. Soc.* **2017**, *139*, 17683−17693.
(84) Johnson, J. A.; Lu, Y. Y.; Burts, A. O.; Lim, Y.-H.; Finn, M. G.; Koberstein, J. T.; Turro, N. J.; Tirrell, D. A.; Grubbs, R. H. Core-Clickable PEG-Branch-Azide Bivalent-Bottle-Brush Polymers by ROMP: Grafting-Through and Clicking-To. *J. Am. Chem. Soc.* **2011**, *133*, 559−566.
(85) Li, Y.; Themistou, E.; Zou, J.; Das, B. P.; Tsianou, M.; Cheng, C. Facile Synthesis and Visualization of Janus Double-Brush Copolymers. *ACS Macro Lett.* **2012**, *1*, 52−56.
(86) Radzinski, S. C.; Foster, J. C.; Matson, J. B. Synthesis of Bottlebrush Polymers via Transfer-to and Grafting-through Approaches Using a RAFT Chain Transfer Agent with a ROMP-Active Z-Group. *Polym. Chem.* **2015**, *6*, 5643−5652.
(87) Kawamoto, K.; Zhong, M.; Gadelrab, K. R.; Cheng, L.-C.; Ross, C. A.; Alexander-Katz, A.; Johnson, J. A. Graft-through Synthesis and Assembly of Janus Bottlebrush Polymers from A-Branch-B Diblock Macromonomers. *J. Am. Chem. Soc.* **2016**, *138*, 11501−11504.
(88) Lohmeijer, B. G. G.; Pratt, R. C.; Leibfarth, F.; Logan, J. W.; Long, D. A.; Dove, A. P.; Nederberg, F.; Choi, J.; Wade, C.; Waymouth, R. M.; et al. Guanidine and Amidine Organocatalysts for Ring-Opening Polymerization of Cyclic Esters. *Macromolecules* **2006**, *39*, 8574−8583.
(89) Walsh, D. J.; Lau, S. H.; Hyatt, M. G.; Guironnet, D. Kinetic Study of Living Ring-Opening Metathesis Polymerization with Third-Generation Grubbs Catalysts. *J. Am. Chem. Soc.* **2017**, *139*, 13644−13647.
(90) Radzinski, S. C.; Foster, J. C.; Chapleski, R. C.; Troya, D.; Matson, J. B. Bottlebrush Polymer Synthesis by Ring-Opening Metathesis Polymerization: The Significance of the Anchor Group. *J. Am. Chem. Soc.* **2016**, *138*, 6998−7004.
(91) Choi, T.-L.; Grubbs, R. H. Controlled Living Ring-Opening-Metathesis Polymerization by a Fast-Initiating Ruthenium Catalyst. *Angew. Chem., Int. Ed.* **2003**, *42*, 1743−1746.
(92) Bird, B. R.; Stewart, W. E.; Lightfoot, E. N. *Transport Phenomena*, 2nd ed; John Wiley & Sons, Inc., 2006.
(93) Shapiro, M.; Brenner, H. Chemically Reactive Generalized Taylor Dispersion Phenomena. *AIChE J.* **1987**, *33*, 1155−1167.
(94) Shapiro, M.; Brenner, H. Taylor Dispersion of Chemically Reactive Species: Irreversible First-Order Reactions in Bulk and on Boundaries. *Chem. Eng. Sci.* **1986**, *41*, 1417−1433.
(95) Codd, S. L.; Manz, B.; Seymour, J. D.; Callaghan, P. T. Taylor Dispersion and Molecular Displacements in Poiseuille Flow. *Phys. Rev. E: Stat. Phys., Plasmas, Fluids, Relat. Interdiscip. Top.* **1999**, *60*, R3491−R3494.
(96) Reissner, E. On the Foundations of Generalized Linear Shell Theory. *Theory of Thin Shells*; Springer Berlin Heidelberg: Berlin, Heidelberg, 1969; Vol. *204*, pp 15−30.
(97) Cottet, H.; Biron, J.-P.; Martin, M. Taylor Dispersion Analysis of Mixtures. *Anal. Chem.* **2007**, *79*, 9066−9073.
(98) Beard, D. A. Taylor Dispersion of a Solute in a Microfluidic Channel. *J. Appl. Phys.* **2001**, *89*, 4667−4669.
(99) Alizadeh, A.; Nieto de Castro, C. A.; Wakeham, W. A. The Theory of the Taylor Dispersion Technique for Liquid Diffusivity Measurements. *Int. J. Thermophys.* **1980**, *1*, 243−284.
(100) Taylor, G. Dispersion of Soluble Matter in Solvent Flowing Slowly through a Tube. *Proc. R. Soc. A Math. Phys. Eng. Sci.* **1953**, *219*, 186−203.
(101) Taylor, G. Conditions under Which Dispersion of a Solute in a Stream of Solvent Can Be Used to Measure Molecular Diffusion. *Proc. R. Soc. A Math. Phys. Eng. Sci.* **1954**, *225*, 473−477.
(102) Hiemenz, P.; Lodge, T. P. *Polymer Chemistry*, 2nd ed.; CRC Press, 2007.
(103) Odian, G. *Principles of Polymerization*; John Wiley & Sons, Inc.: Hoboken, NJ, USA, 2004.
(104) Roberts, G. W. *Chemical Reactions and Chemical Reactors*, 1st ed.; John Wiley & Sons, Inc., 2008.

DOI: 10.1021/acs.macromol.9b00845
Macromolecules 2019, 52, 4847−4857

(105) Nauman, E. B. *Chemical Reactor Design, Optimization, and Scaleup*; John Wiley & Sons, Inc.: Hoboken, NJ, USA, 2008.
(106) Sheiko, S. S.; Sumerlin, B. S.; Matyjaszewski, K. Cylindrical Molecular Brushes: Synthesis, Characterization, and Properties. *Prog. Polym. Sci.* **2008**, *33*, 759−785.
(107) Xia, Y.; Kornfield, J. A.; Grubbs, R. H. Efficient Syntheses of Brush Polymers via Living Ring Opening Metathesis Polymerization of Macromonomers. *Macromolecules* **2009**, *42*, 3761−3766.
(108) Rzayev, J. Molecular Bottlebrushes: New Opportunities in Nanomaterials Fabrication. *ACS Macro Lett.* **2012**, *1*, 1146−1149.
(109) Sheiko, S. S.; Sun, F. C.; Randall, A.; Shirvanyants, D.; Rubinstein, M.; Lee, H.-i.; Matyjaszewski, K. Adsorption-induced scission of carbon-carbon bonds. *Nature* **2006**, *440*, 191−194.
(110) Braunecker, W. A.; Matyjaszewski, K. Controlled/Living Radical Polymerization: Features, Developments, and Perspectives. *Prog. Polym. Sci.* **2007**, *32*, 93−146.
(111) Sheiko, S. S.; Da Silva, M.; Shirvaniants, D.; LaRue, I.; Prokhorova, S.; Moeller, M.; Beers, K.; Matyjaszewski, K. Measuring Molecular Weight by Atomic Force Microscopy. *J. Am. Chem. Soc.* **2003**, *125*, 6725−6728.
(112) Burdyńska, J.; Li, Y.; Aggarwal, A. V.; Höger, S.; Sheiko, S. S.; Matyjaszewski, K. Synthesis and Arm Dissociation in Molecular Stars with a Spoked Wheel Core and Bottlebrush Arms. *J. Am. Chem. Soc.* **2014**, *136*, 12762−12770.
(113) Park, I.; Nese, A.; Pietrasik, J.; Matyjaszewski, K.; Sheiko, S. S. Focusing Bond Tension in Bottle-Brush Macromolecules during Spreading. *J. Mater. Chem.* **2011**, *21*, 8448.
(114) Nese, A.; Li, Y.; Averick, S.; Kwak, Y.; Konkolewicz, D.; Sheiko, S. S.; Matyjaszewski, K. Synthesis of Amphiphilic Poly(N-vinylpyrrolidone)-b-poly(vinyl acetate) Molecular Bottlebrushes. *ACS Macro Lett.* **2011**, *1*, 227−231.
(115) Finnegan, J. R.; He, X.; Street, S. T. G.; Garcia-Hernandez, J. D.; Hayward, D. W.; Harniman, R. L.; Richardson, R. M.; Whittell, G. R.; Manners, I. Extending the Scope of "Living" Crystallization-Driven Self-Assembly: Well-Defined 1D Micelles and Block Comicelles from Crystallizable Polycarbonate Block Copolymers. *J. Am. Chem. Soc.* **2018**, *140*, 17127−17140.
(116) Lord, S. J.; Sheiko, S. S.; LaRue, I.; Lee, H.-I.; Matyjaszewski, K. Tadpole Conformation of Gradient Polymer Brushes. *Macromolecules* **2004**, *37*, 4235−4240.
(117) Xia, Y.; Olsen, B. D.; Kornfield, J. a.; Grubbs, R. H. Efficient Synthesis of Narrowly Dispersed Brush Copolymers and Study of Their Assemblies: The Importance of Side Chain Arrangement. *J. Am. Chem. Soc.* **2009**, *131*, 18525−18532.
(118) Börner, H. G.; Beers, K.; Matyjaszewski, K.; Sheiko, S. S.; Möller, M. Synthesis of Molecular Brushes with Block Copolymer Side Chains Using Atom Transfer Radical Polymerization. *Macromolecules* **2001**, *34*, 4375−4383.
(119) Elli, S.; Ganazzoli, F.; Timoshenko, E. G.; Kuznetsov, Y. A.; Connolly, R. Size and Persistence Length of Molecular Bottle-Brushes by Monte Carlo Simulations. *J. Chem. Phys.* **2004**, *120*, 6257−6267.
(120) Feuz, L.; Leermakers, F. A. M.; Textor, M.; Borisov, O. Bending Rigidity and Induced Persistence Length of Molecular Bottle Brushes: A Self-Consistent-Field Theory. *Macromolecules* **2005**, *38*, 8891−8901.
(121) Khalatur, P. G.; Shirvanyanz, D. G.; Starovoitova, N. Y.; Khokhlov, A. R. Conformational Properties and Dynamics of Molecular Bottle-Brushes: A Cellular-Automaton-Based Simulation. *Macromol. Theory Simulations* **2000**, *9*, 141−155.
(122) Angelescu, D. G.; Linse, P. Monte Carlo Simulations of Multigraft Homopolymers in Good Solvent. *Macromolecules* **2014**, *47*, 415−426.
(123) Maleki, H.; Theodorakis, P. E. Structure of Bottle-Brush Brushes under Good Solvent Conditions: A Molecular Dynamics Study. *J. Phys. Condens. Matter* **2011**, *23*, 505104.
(124) Chatterjee, D.; Vilgis, T. A. Scaling Laws of Bottle-Brush Polymers in Dilute Solutions. *Macromol. Theory Simulations* **2016**, *25*, 518−523.
(125) Paturej, J.; Kreer, T. Hierarchical Excluded Volume Screening in Solutions of Bottlebrush Polymers. *Soft Matter* **2017**, *13*, 8534−8541.
(126) Liang, H.; Cao, Z.; Wang, Z.; Sheiko, S. S.; Dobrynin, A. V. Combs and Bottlebrushes in a Melt. *Macromolecules* **2017**, *50*, 3430−3437.
(127) Saariaho, M.; Ikkala, O.; Szleifer, I.; Erukhimovich, I.; ten Brinke, G. On Lyotropic Behavior of Molecular Bottle-Brushes: A Monte Carlo Computer Simulation Study. *J. Chem. Phys.* **1997**, *107*, 3267−3276.
(128) Saariaho, M.; Ikkala, O.; ten Brinke, G. Molecular Bottle Brushes in Thin Films: An off-Lattice Monte Carlo Study. *J. Chem. Phys.* **1999**, *110*, 1180−1187.
(129) Tsuda, K. Intrinsic Viscosity of Rigid Complex Molecules. *Rheol. Acta* **1970**, *9*, 509−516.
(130) Tsuda, K. Hydrodynamic Properties of Rigid Complex Molecules. *Polym. J.* **1970**, *1*, 616−631.
(131) Garcia De la Torre, J.; Lopez Martinez, M. C.; Tirado, M. M. Monte Carlo Study of Hydrodynamic Properties of Flexible Linear Chains: Analysis of Several Approximate Methods. *Macromolecules* **1984**, *17*, 2715−2722.
(132) Carrasco, B.; García de la Torre, J. Hydrodynamic Properties of Rigid Particles: Comparison of Different Modeling and Computational Procedures. *Biophys. J.* **1999**, *76*, 3044−3057.
(133) Jaeger, H. M.; de Pablo, J. J. Perspective: Evolutionary Design of Granular Media and Block Copolymer Patterns. *APL Mater.* **2016**, *4*, 053209.
(134) Hannon, A. F.; Gotrik, K. W.; Ross, C. A.; Alexander-Katz, A. Inverse Design of Topographical Templates for Directed Self-Assembly of Block Copolymers. *ACS Macro Lett.* **2013**, *2*, 251−255.
(135) Miskin, M. Z.; Khaira, G.; de Pablo, J. J.; Jaeger, H. M. Turning Statistical Physics Models into Materials Design Engines. *Proc. Natl. Acad. Sci.* **2016**, *113*, 34−39.
(136) Lindquist, B. A.; Jadrich, R. B.; Truskett, T. M. Communication: Inverse Design for Self-Assembly via on-the-Fly Optimization. *J. Chem. Phys.* **2016**, *145*, 111101.
(137) Hannon, A. F.; Ding, Y.; Bai, W.; Ross, C. A.; Alexander-Katz, A. Optimizing Topographical Templates for Directed Self-Assembly of Block Copolymers via Inverse Design Simulations. *Nano Lett.* **2014**, *14*, 318−325.

DOI: 10.1021/acs.macromol.9b00845
Macromolecules 2019, 52, 4847−4857